Proceedings of the 3rd International Conference on Green Energy, Environment and Sustainable Development (GEESD2022), X. Zhang et al. (Eds.)

doi:10.3233/ATDE220304

Numerical Simulation of Shear Failure Behavior of Hydrate-Bearing Sediment Using Discrete Element Method

Shuaishuai NIE[a], Chen CHEN[a,b,1] and Jian SONG[c]
[a] *College of Construction Engineering, Jilin University, Changchun 130026, Jilin, China*
[b] *Key Laboratory of Drilling and Exploitation Technology in Complex Conditions, Ministry of Natural Resources, Changchun 130026, Jilin, China*
[c] *Gas Production Plant No.5, PetroChina Changqing Oilfield Company, Xi'an 710018, Shannxi, China*

Abstract. Gas recovery from hydrate-bearing sediments attracts worldwide interest due to the huge reserves of methane there, recognized as a promising future energy resource. However, the mechanical behavior of hydrate-bearing sediment is rarely studied. In this study, the drained shear test on hydrate-bearing sand with different hydrate saturation was simulated using the discrete element method. In particular, the pore habits of hydrate in sands were considered in the simulation, and the meso-failure behavior such as the evolution of contact-force chains and the occurrence of microcracks were thoroughly investigated. In general, the simulations yielded the mechanical response (e.g., deviatoric stress-strain curve) of hydrate-bearing sand similar to the laboratory experiments, and the existence of hydrates plays a crucial role in the failure behavior. It is found that "X-type" shear bands are more likely to form in hydrate-bearing sand with higher hydrate saturation because enough bonds are broken to facilitate microcrack connection. Furthermore, tensile failure, tensile-shear failure, and compression-shear failure exist simultaneously during shearing, of which tensile failure and tensile-shear failure are dominant.

Keywords. Hydrate-bearing sediments, failure behavior, discrete element method, hydrate distribution, shear test

1. Introduction

Natural gas hydrate is considered a promising alternative energy resource due to its wide distribution, huge reserves, cleanliness, and high energy density [1]. It is estimated that approximately 99 % of the hydrates occur in marine sediments, and many challenges need to be addressed before commercial development [2]. Among them, geomechanical challenges are attracting more attention, such as the seabed instability caused by hydrate decomposition and well sand production [3]. The foundation for addressing these issues is to understand the mechanics of hydrate-bearing sediments. Therefore, research on the mechanics of hydrate-bearing sediments has become a hot topic.

[1] Corresponding Author, Chen CHEN, College of Construction Engineering, Jilin University, Changchun 130026, Jilin, China; Email: chenchen@jlu.edu.cn.

Extracting undisturbed samples from the deep-sea bed is technically demanding and costly; thus, many researchers utilized indoor synthetic or reconstruction specimens to study the mechanics of hydrate-bearing sediments and found their mechanical properties were affected by the particle size, morphology, hydrate saturation, stress-state, porosity, etc. [4, 5]. Additionally, several studies attempted to combine micro observations with shear tests to explore the meso-mechanics of hydrate-bearing sediments and detected particle deformation and rotation [6, 7]. However, the requirements of the mechanical test on the sample size exceeded the penetration ability of X-rays; thus, it is challenging to capture the interior failure evolution. At present, the discrete element method (DEM), a particle-scale simulation method, is an effective method to study the meso-mechanics of discontinuous mediums and has been used to study the interaction between hydrate particles and sediments particles [8]. Brugada et al. (2010) found that the existence of pore-filling hydrates enhanced the internal friction angle [9]. Jung et al. (2012) pointed out that hydrate-bearing sediments with patchy hydrate have a lower shear strength, compared to the hydrate-bearing sediments with random hydrate particles [10]. Jiang et al. (2017) established a DEM model considering the cemented bond thickness and found that the shear strength increases as bond thickness increases [11]. Gong et al. (2020) indicated an initial increase in strength then decreased with an increase in the deposition angle [12]. The above research proves DEM is reliable in the simulation of the mechanical response of hydrate-bearing sediments. However, existing studies barely focus on the meso failure behavior of sediments, which is essential for hydrate development.

In this study, a drained shear model of hydrate-bearing sand (HBS) was established based on the DEM, and the model was verified by comparing the stress-strain curves of simulation and experiment. Furthermore, the meso-mechanical characteristics, including contact-force chains, and deviatoric stress contribution were investigated, and the failure mechanism was obtained by monitoring the generation of microcracks, the failure mode of bonds, and the evolution of shear bands. These findings provide fundamental support for addressing geomechanical issues in hydrate development.

2. Modeling

Particle flow code developed based on the DEM is employed in this study, in which the material is regarded as rigid particle aggregates, and a time-stepping algorithm is used for the calculation of the force-displacement and particle movement [13].

2.1. Specimen Preparation

The sand particles were generated based on the Toyoura sand particle gradation curve (Figure 1a), and smaller particles (0.04 mm) were used to represent hydrates. The density of sand and hydrate was 2650 kg/m^3 and 320 kg/m^3, respectively.

Previous studies have found that hydrates are preferentially formed at the gas-water interface, i.e., hydrates gradually grow from the sand surface into pores [14]. Thus, the following steps were adopted to simulate the pore habits of hydrates: firstly, one hydrate particle with a diameter of 0.01 mm was randomly generated in the pores. Further, all the contacts of the hydrate particles were trawled. If the sand-hydrate (s_h) contact type exists, remaining the hydrate particle. Otherwise, deleting the hydrate particle to ensure that the hydrate was initially generated on the sand. The above process was repeated until reached the predetermined hydrate saturation. Finally, hydrate particles were amplified using the gradual expansion method to stimulate the growth of hydrate. The expansion rate is 0.0005. After each expansion, 10,000 steps were performed to reduce the overlap. Figure 1b shows the DEM model of HBS, in which the yellow and blue particles represent sand and hydrates, respectively. It can be seen that hydrates grow from the sand surface into pores as hydrate saturation increases. Therefore, the pore habits of hydrate in real samples is well simulated in the DEM model with this method.

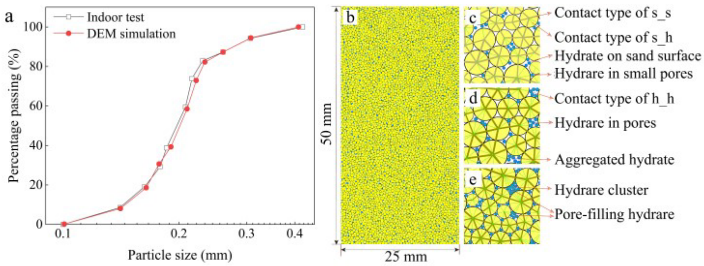

Figure 1. (a) Particle size distribution of sand; (b) DEM model of HBS.

2.2. Contact Models

There are 3 contact types in HBS, i.e, sand-sand (s_s), sand-hydrate (s_h), and hydrate–hydrate (h_h). Previous studies have found that hydrate cemented sand in the specimen; thus, there are bonds in s_h and h_h and no bond in s_s. For s_s, a rolling resistance model was adopted to simulate the interlocking effect of sand, in which the rolling resistance coefficient is used to characterize the shape effect of sand [13]. For s_h and h_h, a parallel bond model was used. Previous studies have proved the applicability of the parallel bond model in the simulation of HBS [11, 12].

2.3. Model Parameters

The calibration method is commonly used in DEM modeling, i.e., testing the mechanical properties of particle aggregates, and then calibrating the values of meso mechanical parameters until the macro mechanical response obtained by the DEM is consistent with the real data. In this study, the values of meso parameters were calibrated based on the experimental results of Masui et al. (2005) [5], as shown in Table 1.

Table 1. Model parameters.

Contact type	s_s	s_h	h_h
Effective modulus (N)	8.0e8	8.0e7	8.0e7
Normal-to-shear stiffness ratio	1.5	1.5	1.5
Friction coefficient	0.37	0.04	0.04
Rolling resistance coefficient	6.0	_	_
Bond effective modulus (N)	_	1.0e7	1.0e7
Bond normal-to-shear stiffness ratio	_	1.5	1.5
Gap interval (m)	_	1.0e-6	1.0e-6
Tensile strength (N)	_	3.6e6	3.6e6
Cohesion (N)	_	3.6e6	3.6e6
Friction angle (°)	_	10	10

2.4. Model Validation

Figure 2 shows the experimental and simulated deviatoric stress, volumetric strain, and axial strain. It can be seen that the mechanical response of HBS obtained by simulation is similar to that of laboratory experiments. Specifically, with the increase in hydrate saturation, the maximum deviatoric stress and shear modulus increase, and the strain-softening and the dilatancy effect are more evident.

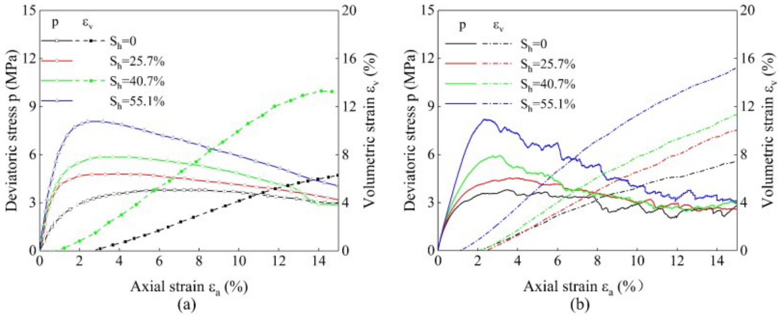

Figure 2. (a) Experimental; (b) simulated deviatoric stress, volumetric strain, and axial strain.

3. Results and Discussion

3.1. Evolution of Contact-Force Chains

Contact-force chain is a form of contact force between particles and reflects the transfer path of the external load. Figure 3 shows the contact-force chains in the HBS with hydrate saturation of 40.7%, where the widths of the chains represent the values of the contact force. Before loading, the contact-force chains presented a uniform circular distribution, indicating that the HBS was homogeneous. After the HBS was compressed, the contact-force chains deflected in the axial direction to bear the load, with a gradual increase in the contact force. At the maximum deviatoric stress, the contact-force chains became more orderly. Subsequently, the contact force was reduced and local contact-force chains become sparse and disordered as the HBS is damaged.

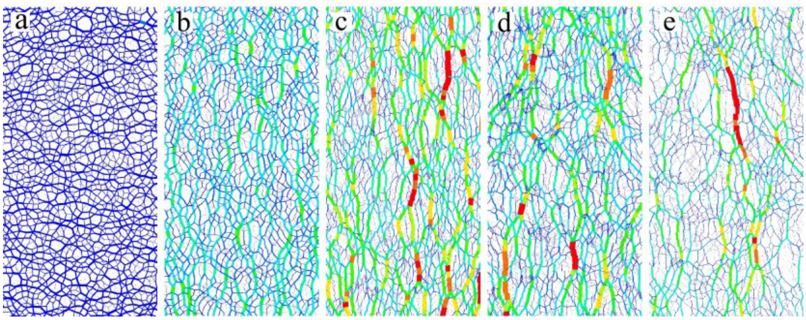

Figure 3. (a) Contact-force chains in HBS at axial strain of 3%; (b) Contact-force chains in HBS at axial strain of 6%; (c) Contact-force chains in HBS at axial strain of 9%; (d) Contact-force chains in HBS at axial strain of 12%; (e) Contact-force chains in HBS at axial strain of 15% .

3.2. Deviatoric Stress Contribution of Different Contacts

The deviatoric stress contribution can be obtained by decomposing the contact force of different contact types along the loading direction. As shown in Figure 4a, at the maximum deviatoric stress, the deviatoric stress contribution of s_s increases as hydrate saturation increases, and the contribution ratio decreases. For s_h, deviatoric stress contribution and contribution ratio increase as hydrate saturation increases, indicating that part of hydrates attached to the sand can be regarded as skeleton particles. For h_h, deviatoric stress contribution and contribution ratio below 0.25 MPa and 5% when hydrate saturation is lower than 40.7%, respectively. However, when hydrate saturation is 55.1%, deviatoric stress contribution and contribution ratio reach 1.07 MPa and 13%, respectively. This is because the hydrate masses gathered in the macropores can be regarded as frame support, thus significantly enhancing the deviatoric stress of hydrates.

At residual deviatoric stress (corresponding to the axial strain of 12%, Figure 4b), the order of the deviatoric stress contribution is unchanged. However, compared with the contribution ratio at the maximum deviatoric stress, the contribution ratio of s_h and h_h is higher. When hydrate saturation is 55.1%, the total contribution ratio of s_h and h_h reaches 51%, which exceeds the contribution ratio of s_s. This indicates that the failure of HBS weakens the bearing capacity of the sand skeleton.

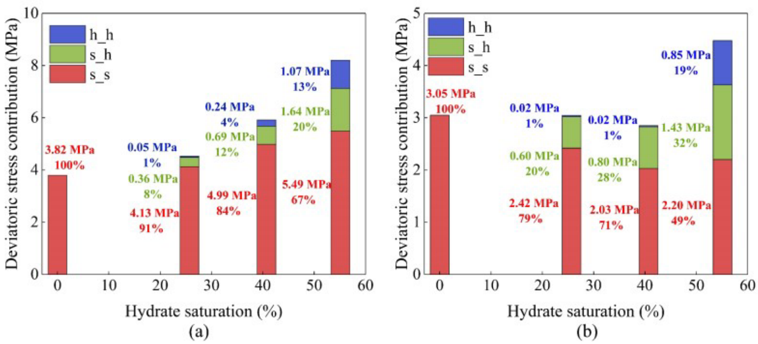

Figure 4. (a) Deviatoric stress contribution at maximum deviatoric stress; (b) Deviatoric stress contribution at residual deviatoric stress.

3.3. Evolution of Microcracks

The number of microcracks developed within 0.05 % of axial strain was monitored and recorded as acoustic emission (AE) events, and the failure modes (tensile, compression-shear, tensile-shear failure) of the bonds (s_h and h_h) were judged, and the number of microcracks generated by different failure modes was counted, as shown in Figure 5. The evolution of AE events presents three stages. The first (axial strain < 3%) is the crack initiation stage, and a small number of microcracks are generated. In the second stage of crack development (3% < axial strain < 8%), the AE events reached the maximum. The third (axial strain > 8%) is the crack decay stage, Here, the AE events attenuate and finally stabilize. When hydrate saturation is 25.7% (Figure 5a), s_h is dominated by tensile failure, accompanied by a small amount of tensile-shear and compression-shear failure. For h_h, tensile failure is also dominant, while shear failure barely appears. Comparing the failure modes in HBS with different hydrate saturation (Figures 5a-5c), it found that the dominant failure mode of s_h and h_h is also the tensile failure. This is because there is dilatancy in HBS during shearing, which induces large tensile stress perpendicular to the loading direction. Additionally, the number of tensile microcracks (h_h) significantly increased when the hydrate saturation is 55.1%, indicating the HBS with high hydrate saturation is controlled by the tensile failure of s_h and h_h.

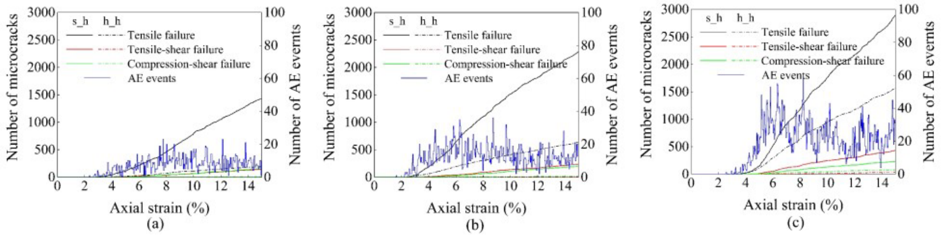

Figure 5. (a): The number of AE events and microcracks in HBS with hydrate saturation of 25.7%; (b): The number of AE events and microcracks in HBS with hydrate saturation of 40.7%; (c): The number of AE events and microcracks in HBS with hydrate saturation of 55.1%.

3.4. Evolution of Shear Bands

To observe the distribution of shear bands, the HBS was covered with the measuring circles. Then the number of cracks in each measuring circle was counted to obtain a hot spot map of cracks, as shown in Figure 6. For hydrate saturation of 25.7%, microcracks were mostly distributed in the upper right and lower left areas of the HBS along the 60° and 120° angles. For hydrate saturation of 40.7%, two conjugate shear bands appeared, one extending from the upper left to the lower right and the other extending from the upper right to the lower left, similar to an "X" shape. For hydrate saturation of 55.1%, five shear bands were connected to form multiple X-shaped shear bands, indicating that the explosive break of bonds is sufficient to promote the connection of microcracks. This revealed the strain-softening behavior of the HBS with high hydrate saturation, i.e., the macro shear band weakened the bearing capacity of HBS.

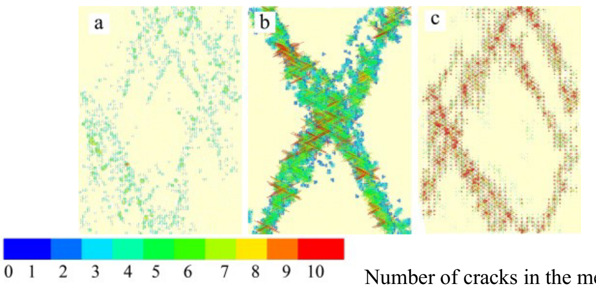

Number of cracks in the measuring circle

Figure 6. (a): Shear bands in HBS with hydrate saturation of 25.7%; (b): Shear bands in HBS with hydrate saturation of 40.7%; (c): Shear bands in HBS with hydrate saturation of 55.1%.

4. Conclusion

In this study, the biaxial shear test of HBS was simulated using DEM, and the deviatoric stress contribution and failure mode of bonds, as well as the evolution of macro shear bands, were investigated. The major conclusions are as follows:

(1) The pore habits of hydrates play a crucial role in the mechanical response of HBS. For hydrate saturation of 25.7%, hydrates scattered adhering to the sand, which barely bears the load. With hydrate saturation increases, the gathered hydrates play the role of bridge and frame, thus significantly enhancing the strength of HBS. Moreover, s_h has a greater deviatoric stress contribution than h_h, e.g., the contribution ratio of s_h and h_h is 32% and 19% when the hydrate saturation is 55.1%, respectively.

(2) Tensile failure and shear failure exist simultaneously in HBS during shearing, and tensile failure is the main one, which is consistent with the dilatancy phenomenon in HBS. When the hydrate saturation is lower than 40.7%, the hydrate particles attached to sand will fall off due to the tensile or shear stress, thus microcracks are mainly generated between the hydrate particles and the sand particles. When the hydrate saturation reaches 55.1%, the gathered hydrate particles are separated due to the rotation of particles, and more microcracks are generated inside hydrate clusters.

(3) The number of microcracks increases significantly as the hydrate saturation increases, and “X” conjugate shear bands similar to rock-like are formed. This finding explains the brittle failure behavior of HBS with high hydrate saturation. For hydrate saturation of 25.7%, microcracks are scattered along with the shear angles of 60° and 120°, and no shear bands can be formed. When hydrate saturation reaches 40.7%, microcracks are connected and an X-type conjugate shear band is formed.

References

[1] Kvenvolden KA. Methane hydrate—A major reservoir of carbon in the shallow geosphere? Chemical Geology. 1988;71(1-3):41-51.

[2] Klauda JB, Sandler SI. Global distribution of methane hydrate in ocean sediment. Energy & Fuels. 2005;19(2):459-70.

[3] Nie S, Zhong X, Ma Y, Pan D, Liu K, Wang Y, et al. Numerical simulation of a new methodology to exploit challenging marine hydrate reservoirs without impermeable boundaries. Journal of Natural Gas Science and Engineering. 2021;96.

[4] Ghiassian H, Grozic JLH. Strength behavior of methane hydrate bearing sand in undrained triaxial testing. Marine and Petroleum Geology. 2013;43:310-9.

[5] Masui A, Haneda H, Ogata Y, Aoki K. Effects of methane hydrate formation on shear strength of synthetic methane hydrate sediments. Proceedings of the International Offshore and Polar Engineering Conference. 2005;15:364-9.

[6] Yoneda J, Jin Y, Katagiri J, Tenma N. Strengthening mechanism of cemented hydrate-bearing sand at microscales. Geophysical Research Letters. 2016;43(14):7442-50.

[7] Seol Y, Lei L, Choi JH, Jarvis K, Hill D. Integration of triaxial testing and pore-scale visualization of methane hydrate bearing sediments. Rev Sci Instrum. 2019;90(12):124504.

[8] Cundall PA, Strack ODL. A discrete numerical model for granular assemblies. Geotechnique. 1979;29:47-65.

[9] Brugada J, Cheng YP, Soga K, Santamarina JC. Discrete element modelling of geomechanical behaviour of methane hydrate soils with pore-filling hydrate distribution. Granular Matter. 2010;12(5):517-25.

[10] Jung J-W, Santamarina JC, Soga K. Stress-strain response of hydrate-bearing sands: Numerical study using discrete element method simulations. Journal of Geophysical Research: Solid Earth. 2012;117(B4).

[11] Jiang M, He J, Wang J, Zhou Y, Zhu F. Discrete element analysis of the mechanical properties of deep-sea methane hydrate-bearing soils considering interparticle bond thickness. Comptes Rendus Mécanique. 2017;345(12):868-89.

[12] Gong B, Jiang Y, Yan P, Zhang S. Discrete element numerical simulation of mechanical properties of methane hydrate-bearing specimen considering deposit angles. Journal of Natural Gas Science and Engineering. 2020;76.

[13] Inc ICG. PFC2D-Particle Flow Code in two dimensions. Ver. 4.0. User's ManualICG, Minneapolis. 2010.

[14] Chaouachi M, Falenty A, Sell K, Enzmann F, Kersten M, Haberthür D, et al. Microstructural evolution of gas hydrates in sedimentary matrices observed with synchrotron X-ray computed tomographic microscopy. Geochemistry, Geophysics, Geosystems. 2015;16(6):1711-22.